Advanced Powder Technology 27 (2016) 2005–2011

Contents lists available at ScienceDirect

Advanced Powder Technology

journal homepage: www.elsevier.com/locate/apt

Original Research Paper

Fabrication of *c*-axis oriented Si_3N_4 ceramics using multilayered-graphene-coated β-Si_3N_4 seeds and their orientation in an innovative low magnetic field

Takuma Takahashi [a,*], Mariko Sado [b], Nanako Sugimoto [b], Junichi Tatami [b], Motoyuki Iijima [b], Satoshi Inagaki [b], Yoshihiro Kubota [b], Isao Yamamoto [b], Satoshi Tanaka [c]

[a] Kanagawa Academy of Science and Technology, KSP, 3-2-1 Sakado, Takatsu-ku, Kawasaki, Kanagawa 213-0012, Japan
[b] Yokohama National University, 79-7, Tokiwadai, Hodogaya-ku, Yokohama, Kanagawa 240-8501, Japan
[c] Nagaoka University of Technology, 1603-1 Kamitomioka Nagaoka, Niigata 940-2188, Japan

ARTICLE INFO

Article history:
Received 31 March 2016
Received in revised form 14 June 2016
Accepted 6 July 2016
Available online 3 August 2016

Keywords:
Silicon nitride
Magnetic field orientation
Graphene
Thermal conductivity

ABSTRACT

c-axis oriented Si_3N_4 ceramics were fabricated by applying a low static magnetic field. Conventionally, *c*-axis oriented Si_3N_4 ceramics are fabricated using a rotating magnetic field of over 10 T considering the anisotropy and the magnitude of diamagnetic susceptibility between *c*- and *a*-axes. In this work, multilayered-graphene was used for orienting rod-like β-Si_3N_4 particles as graphene exhibits a high diamagnetic anisotropy. The multilayered-graphene was coated with their orientation on the surface of rod-like β-Si_3N_4 particles by using a mechanical treatment process. As a result, the *c*-axis of multilayered-graphene-coated β-Si_3N_4 particles were oriented parallel direction to the applied magnetic field even at 0.4 T. In addition, *c*-axis oriented Si_3N_4 ceramics were fabricated successfully by adding a small quantity of multilayered-graphene-coated β-Si_3N_4 particles as seeds. The thermal conductivity of the *c*-axis oriented Si_3N_4 ceramics prepared with a magnetic field of 0.4 T exhibited anisotropy with a higher value achieved in the *c*-axis oriented direction.

1. Introduction

Silicon nitride (Si_3N_4) exhibits promising intrinsic thermal and mechanical properties [1–11]. Si_3N_4 is expected to be applied as a heat sink in silicon carbide (SiC) power devices [12]. SiC power devices are used in various electrical products, such as electric vehicles at high temperatures (above 250 °C) [13]. High thermal conductivity is desired in the thickness direction of the substrate used in SiC power devices. Si_3N_4 exhibits a high thermal conductivity in the *c*-axis direction owing to its crystal anisotropy [14,15]. Hirosaki et al. reported the theoretical thermal conductivity of Si_3N_4 to be 450 and 170 W m^{-1} K^{-1} along the *c*- and *a*-axis directions, respectively [14]. Li et al. demonstrated experimentally the thermal conductivity in an elongated Si_3N_4 grain to be 180 and 69 W m^{-1} K^{-1} in the *c*- and *a*-axis directions, respectively [15]. These results suggest that the *c*-axis orientation of Si_3N_4 grains should be effective in attaining high thermal conductivity. Watari et al. fabricated crystal-orientated Si_3N_4 ceramics using a tape casting technique and hot isostatic pressing [16]. In their technique, β-Si_3N_4 single crystalline particles were added as seed particles with the length of the β-Si_3N_4 particles oriented along the tape-casting direction. The thermal conductivity of the grain-oriented Si_3N_4 sheet along the tape-casting direction at room temperature was found to be 155 W m^{-1} K^{-1}. It is impossible that elongated β-Si_3N_4 particles are aligned to the thickness direction of the sheet. In order to orient β-Si_3N_4 particles, Li et al. have been reported firstly the fabrication of the *c*-axis oriented Si_3N_4 ceramics by using a magnetic field [17]. Zhu et al. reported *c*-axis-oriented Si_3N_4 ceramics fabricated using a rotating magnetic field [18–20] and they reviewed the textured Si_3N_4 ceramics fabricated by applying a stress or a magnetic field [21]. They recently, Zhu et al. reported the whiskers were highly oriented using a rotating magnetic field of 12 T and subsequent sintering [20]. As a result, the obtained *c*-axis-oriented Si_3N_4 ceramics exhibited a high thermal conductivity of 176 W m^{-1} K^{-1}. However, the use of a superconducting magnet suppressed the industrial applications of this material because of small area of the magnet.

Particle orientation in the magnetic field results from the difference in the magnetizing energy between crystal axes, which is given by the following equation [22,23],

* Corresponding author.
E-mail address: takahashi-t@ynu.ac.jp (T. Takahashi).

http://dx.doi.org/10.1016/j.apt.2016.07.006

$$\Delta E = -\frac{1}{2\mu_0}\Delta\chi B^2 V \cdots \quad (1)$$

where ΔE is the anisotropic magnetization energy, μ_0 is the space permeability, $\Delta\chi$ is the difference of magnetic susceptibility in each crystal axis, B is the magnetic flux density, and V is the volume of the spherical particle. Since $\Delta\chi$ is usually small in the range of 10^{-8}–10^{-10} emu/g for diamagnetic materials [24], the orientation of particles needs a strong magnetic field such as 10–12 T. It is well known that graphene, multilayered-graphene, and graphite having a stacking structure of graphene exhibit high diamagnetic susceptibility with a high anisotropy, $\Delta\chi = 2.0 \times 10^{-5}$ emu/g [24]. In graphite, the diamagnetic susceptibility of the *c*-axis direction is much larger than that of the *a*-axis [25]. Therefore, it can be predicted that the *c*-axis direction of graphite orients easily normal to an applied magnetic field even at very low magnetic field. If a particle with an anisotropic shape such as a rod-like β-Si_3N_4 particle is coated by multilayered-graphene with their orientation, the *c*-plane of multilayered-graphene-coated on the surface of particle should be able to orient with particle normal to an applied low static magnetic field owing to the high anisotropic magnetic susceptibility of graphene.

It can be considered that the multilayered-graphene-coated particles are prepared by a mechanical treatment process. The mechanical treatment process has been reported to be useful for preparing various nanocomposite particles [26–31]. In this process, an external mechanical force, specifically a consolidation shear stress, is applied between particles.

In this work, we investigate the fabrication of *c*-axis oriented Si_3N_4 ceramics by molding in a low static magnetic field using multilayered-graphene-coated β-Si_3N_4 nanocomposite particles as seeds for developing the microstructure.

2. Material and methods

2.1. Preparation of multilayered-graphene-coated β-Si_3N_4 particle

α-Si_3N_4 (SN-E10, Ube Industry, Co., Ltd., Japan) and Y_2O_3 (RU-P, Shin-Etsu Chemical, Co., Ltd., Japan) raw powders were used to synthesize rod-like β-Si_3N_4 particles. It has been reported that Y_2O_3 is one of conventional sintering aids to grow β-Si_3N_4 grain during sintering, but Y_2O_3 additive cannot by itself densify Si_3N_4 [32,33]. The composition of mixed powder was α-Si_3N_4:Y_2O_3 = 95:5 at weight ratio. These powders were mixed by ball-milling for 48 h using sialon balls (5 mm diameter) and silicon nitride pot (400 cm^3) in ethanol. As the dispersant, polycarboxylic acid (E503, Chukyo yushi Co., Ltd., Japan) was used in this study is a typical dispersant to disperse α-Si_3N_4 and Y_2O_3 in ethanol [34]. After drying, mixed powder was sintering at 1600 °C for 1 h and at 1900 °C for 2 h in 0.9 MPa of N_2 using an electric furnace (Himulti 5000, Fujidenpa Kogyo Co., Ltd., Japan). The obtained powder was milled after corroding the glassy phase between the particles in HNO_3 as the synthetic powder consisted of many aggregates. Y^{3+} in glassy phase is easily dissolved into the acid to weaken the grain boundary glassy phase [35], which should make pulverization of the aggregated rod-like β-Si_3N_4 easy.

The synthesized β-Si_3N_4 particles (80 vol%) and commercial multilayered-graphene (G-13L, EM Japan, Co., Ltd., Japan; 20 vol %) were used for preparing multilayered-graphene-coated β-Si_3N_4 particles. They were pre-mixed and mechanically treated at 600 W for 10 min in the chamber of a mechanofusion equipment (Nobiluta mini, Hosokawa micron, Co., Ltd., Japan) with the consolidation shear stress. The total volume of the mixed raw powders was 20 cm^3.

2.2. Formation and sintering of green compacts

Y_2O_3 is one of conventional sintering aids to grow β-Si_3N_4 grain during sintering, but only Y_2O_3 is not good to densify Si_3N_4. Furthermore, Y^{3+} is easily dissolved into acid to weaken the grain boundary glassy phase. This is an important point to synthesize β-Si_3N_4 seed particles because the dense Si_3N_4 ceramics are difficult to be separated into individual grain. This is the reason for using Y_2O_3 to make rod-like β-Si_3N_4. On the other hand, Li et al. have been reported that Y_2O_3-HfO_2-SiO_2 system can improve not only enhancement of the densification of Si_3N_4 but also formation of c-HfO_2 crystalline phases to reduce grain boundary glassy phase [36]. Therefore, the Si_3N_4-Y_2O_3-HfO_2-SiO_2 system should be expected to achieve high thermal conductivity. An aqueous slurry containing multilayered-graphene-coated β-Si_3N_4, α-Si_3N_4 (SN-E10, Ube Industry, Co., Ltd., Japan), Y_2O_3 (RU-P, Shin-Etsu Chemical, Co., Japan), HfO_2 (HF001PB, Kojundo Chemical Laboratory Co., Ltd., Japan), and SiO_2 (SO-C2, Admatechs Co., Ltd., Japan) powders were prepared using polyethylene imine (M_w = 10,000) as the dispersant. Zhu et al. have reported that polyethylene imine (PEI) is an effective additive to disperse these powders in aqueous system [37]. In addition, Jang et al. have reported that PEI is also useful to disperse carbon nanotube in aqueous system [38]. Therefore, we used PEI to make an aqueous suspension in this study.

The starting composition was fixed at β-Si_3N_4:α-Si_3N_4:Y_2O_3:HfO_2:SiO_2 = 10:82:2.5:5:0.5 by weight. The dispersion was achieved by mixing for 30 min using an ultrasonic homogenizer. The slurry with a concentration of 20 vol% was placed in plastic molds of 25 mm diameter followed by drying in a static magnetic field from 0.4 to 10 T to prepare particle-oriented green compacts. These compacts were calcined at 700 °C for 3 h in air to burn out the polymer dispersants followed by sintering at 1900 °C for 6 h in 0.9 MPa N_2 in order to densify and grow β-Si_3N_4 grains.

2.3. Measurement and evaluation of properties

Particle size, the length of long and short axes of synthesized β-Si_3N_4 seed particles and β-Si_3N_4 grains after sintering were measured from SEM photographs by image analysis. The length of the long axis was defined as the maximum distance between two points on the edge of the grain. Their average values were calculated using the data over one hundred grains. The length of the short axis was the maximum length normal to the long axis. The orientation of Si_3N_4 ceramics was examined using X-ray diffraction (XRD; MultiFlex 2 kW, Rigaku Co., Japan). The morphologies of particle and the microstructure were observed using a scanning electron microscope (SEM; JSM-6390LV, JEOL, Japan and SU8200, Hitachi High-Technologies, Japan). The compositions of the specimens were analyzed by energy dispersive X-ray spectrometry (EDS; JSM-5200, JEOL, Japan). A scanning probe microscope (SPA400, SII NanoTechnology Inc., Japan) was used to analysis the morphology of the multilayered-graphene on the β-Si_3N_4 particles. Nitrogen adsorption–desorption measurements were carried out at 77 K using a gas adsorption analyzer (BELSORP-mini II, MicrotracBEL, Japan). The specific surface area was estimated using the Brunauer-Emmett-Teller (BET) method. Raman spectroscopy (inVia Reflex, JEOL, Japan) measurements were performed for evaluating the crystallinity of graphene. The relative density was measured using the Archimedes method. The theoretical density was calculated from the composition of the raw powders.

Thermal diffusivity α was measured using a laser flash method (TC-9000H, ULVAC, Japan) at room temperature. Thermal conductivity κ was calculated as the following equation;

$$\kappa = \alpha \cdot \rho \cdot C_p$$

where ρ is the density and C_p is the specific heat capacity of Si_3N_4. In this study, C_p was set to 0.68 J mol^{-1} K^{-1} [39] to calculate the thermal conductivity. We add the procedure to measure the thermal conductivity to the manuscript.

3. Results and discussion

3.1. Morphology of multilayered-graphene-coated β-Si_3N_4 particles

Fig. 1 shows the morphology of synthesized β-Si_3N_4 particles and commercial multilayered-graphene. From the SEM images, the average aspect ratio and particle sizes in the short and long axes of the β-Si_3N_4 particles are found to be 3.8, 5.0, and 1.3 μm, respectively. As the values included in a release book, average thickness and lateral length of a graphene sheet are 60 nm and 3–7 μm, respectively. Fig. 2 shows EDS images of carbon in the β-Si_3N_4 and multilayered-graphene powder mixture prepared by mechanical treatment. In Fig. 2, smaller particles were observed on the elongated β-Si_3N_4 particles. From the EDS analysis, carbon and silicon signals were observed in the same area, implying that carbon exists on the Si_3N_4 particles. Although the details of these smaller particles have not estimated yet, they are probably debris formed by wear of β-Si_3N_4 seeds or multilayered graphene because of compressive and share stress in mechanical treatment process. Fig. 3 shows back scattered electron images of the graphene-coated β-Si_3N_4 seeds observed using a low acceleration voltage in field emission SEM (FE-SEM). Fig. 3(a) and (b) correspond to the topographic images and (c) and (d) show the composition images. A contrast difference is observed on the surface of elongated β-Si_3N_4 seeds as shown in Fig. 3(c) and (d). The brighter and darker regions should correspond to Si_3N_4 and carbon, respectively. Peeling could be observed in Fig. 3(b); however, it is not evident from the contrast difference in Fig. 3(d), indicating that a thin layer consisting of light elements is peeled off. From these results, it can be considered that the peeling was the edge of multilayered-graphene and it was coated on the β-Si_3N_4 particles.

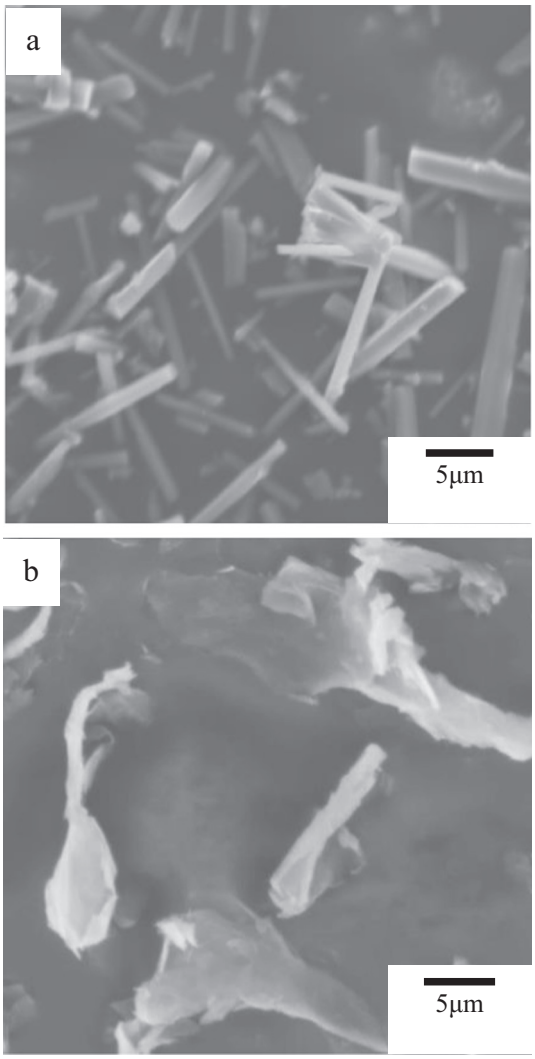

Fig. 1. Morphology of (a) synthesized β-Si_3N_4 particles and (b) commercial graphene flakes.

Fig. 4(a) shows the topographic images of the multilayered-graphene-coated β-Si_3N_4 particle surface observed using the dynamic force microscopy (DFM) mode in the scanning probe microscope. The surface of the multilayered-graphene-coated Si_3N_4 is rough because of the coating with multilayered-graphene particles. Fig. 4(b) and (c) shows the surface profiles of A-A′ and β-B′ indicated in Fig. 4(a), respectively. In Fig. 3(b) and (c), the coating particles exhibit heights of 10–70 nm and width of several hundred nanometers. Considering the initial size of the raw multilayered-graphene particles shown in Fig. 1(b), these coated particles are formed from broken multilayered-graphene. From these geometry differences, the raw multilayered-graphene particles are assumed to break and peel off from the coating on the surface of β-Si_3N_4 during the mechanical treatment process. Fig. 5 shows the Raman spectra of the raw multilayered-graphene and the multilayered-graphene-coated particles. The G and D Raman bands of multilayered-graphene are observed in both the samples. Furthermore, the peak intensity of the G band is high in both the samples, implying a good crystallinity of graphene on the Si_3N_4 particles as similar to that of the raw material. The specific surface area of the mixed powder consisting of synthesized β-Si_3N_4 and multilayered-graphene changes from 9.3 to 4.3 m^2 g^{-1} before and after the mechanical treatment process, which could be attributed to the coating of multilayered-graphene on the surface of β-Si_3N_4 particles.

3.2. Fabrication of c-axis oriented Si_3N_4 ceramics by adding graphene-coated β-Si_3N_4 seeds

Fig. 6 shows SEM image of multilayered-graphene-coated β-Si_3N_4 particles in a low static magnetic field prepared by drying

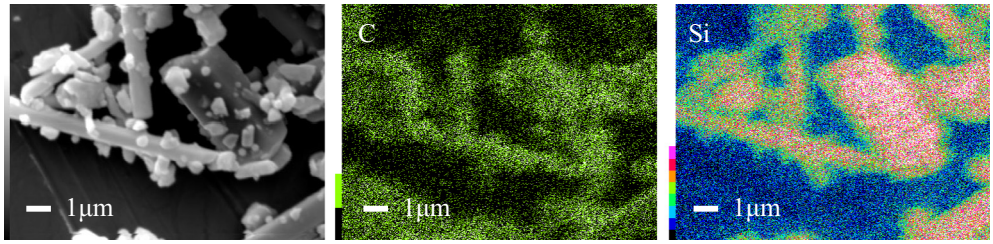

Fig. 2. EDS images of morphology of multilayered-graphene-coated β-Si_3N_4 seeds.

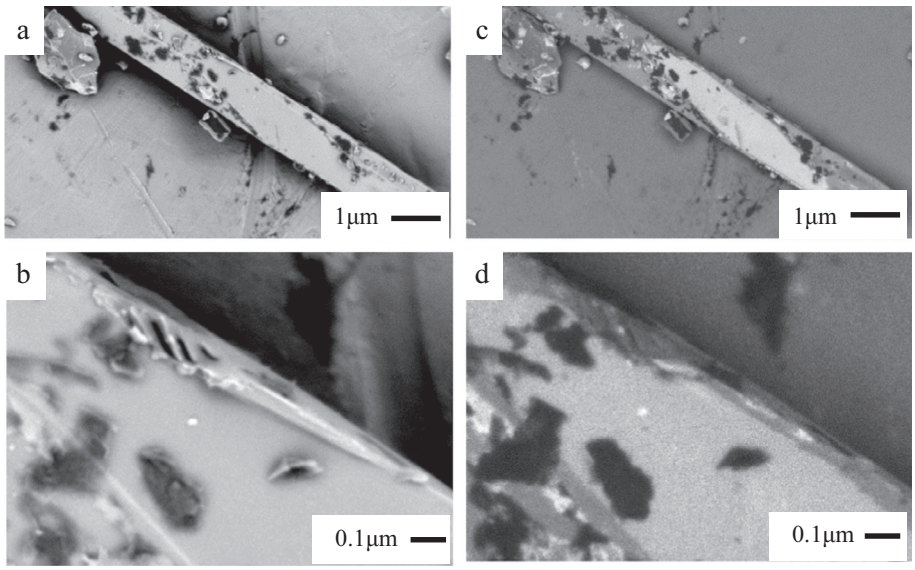

Fig. 3. Back scattered electron images of morphology of graphene coated β-Si_3N_4 seeds (a) and (b) are topographic image, (c) and (d) are composition image.

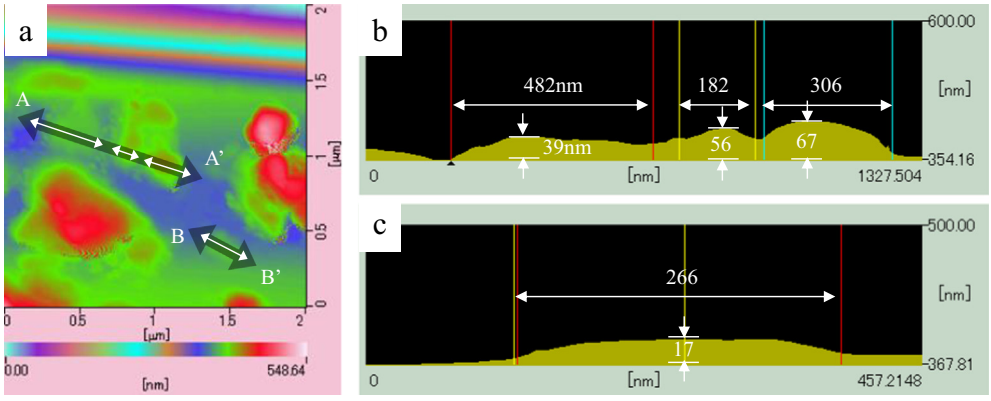

Fig. 4. DFM images of surface of graphene coated β-Si_3N_4 seeds (a) is topographic image, (b) and (c) are cross section image.

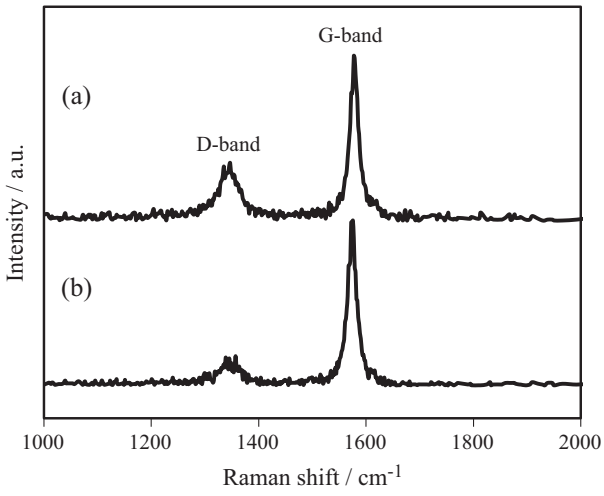

Fig. 5. Raman spectra of (a) graphene on the β-Si_3N_4 particle and (b) raw graphene powder.

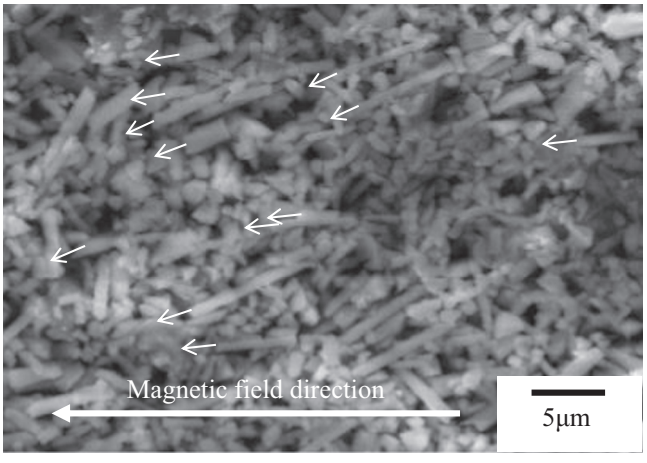

Fig. 6. Orientation of graphene coated β-Si_3N_4 seeds in low static magnetic field.

a drop of the sample dispersed in distilled water in a low static magnetic field of 0.4 T. Most multilayered-graphene-coated β-Si_3N_4 particles are oriented in a direction parallel to the applied magnetic field. Since the β-Si_3N_4 particles alone could not be oriented to a static magnetic field of 0.4 T, we assume that the orientation could be attributed to the $\Delta\chi$ of the coated multilayered-graphene particles.

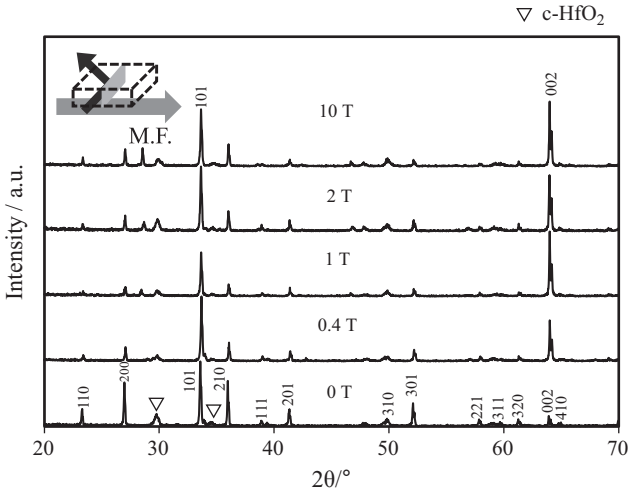

Fig. 7. XRD patterns of Si_3N_4 ceramics including β-Si_3N_4 seed particles (α = 4.4) prepared at from 0 to 10 T.

Fig. 7 shows XRD patterns of the *c*-axis oriented Si_3N_4 ceramics prepared by changing the magnetic field from 0.4 T to 10 T. The plane measured was normal to the applied magnetic field. The intensity of (002) peak increased markedly and the intensities of other peaks derived from (*hk*0) plane decreased definitely in the ceramics prepared with a magnetic field compared with Si_3N_4 ceramics prepared without a magnetic field. Especially, the *c*-axis oriented β-Si_3N_4 particles are obtained even at 0.4 T by using Nd magnets. If settling has effect on the orientation, although Si_3N_4 ceramics prepared without a magnetic field should in-plane orients, but the uniaxial axis orientation is impossible. In fact, no orientation was observed in the case of non-oriented Si_3N_4 ceramics, indicating that the superconducting magnet is not necessary for orientating β-Si_3N_4 particles after coating them with multilayered-graphene particles. However, the *c*-axis orientation lowered in the ceramics prepared with high magnetic field, especially at 10 T. The lower orientation at high magnetic field results from the orientation of small quantity (~5 wt% as the value included in a release book) of β-Si_3N_4 particles included in raw α-Si_3N_4 powder.

Fig. 8 shows the microstructures of the *c*-axis oriented Si_3N_4 ceramics prepared in a magnetic field of 1 T and sintered at 1900 °C for 6 h in 0.9 MPa N_2 observed by using SEM.

Dense oriented structures which are completely different are observed in both the images. In the plane normal to the magnetic field as shown in Fig. 8(a), most particles exhibit a hexagonal shape. In the plane parallel to the magnetic field as shown in Fig. 8(b), most particles exhibit elongated shapes and are oriented in a direction along the applied magnetic field, which is in agreement with the results obtained with the XRD patterns shown in Fig. 7. Fig. 9 illustrates the mechanism of formation of the *c*-axis-oriented structure during sintering. In the sintering process of Si_3N_4, the α-β phase transition and grain growth of β-Si_3N_4 occur by mass diffusion via liquid phase derived from the reaction between SiO_2 on the surface of α-Si_3N_4 and R_2O_3 added as sintering aid. First, the α-β phase transition occurs in the temperature range of 1400–1500 °C. The α-Si_3N_4 particles dissolve into the liquid phase, and then precipitate as very fine β-Si_3N_4 nucleuses at high temperature followed by the densification and grain growth of

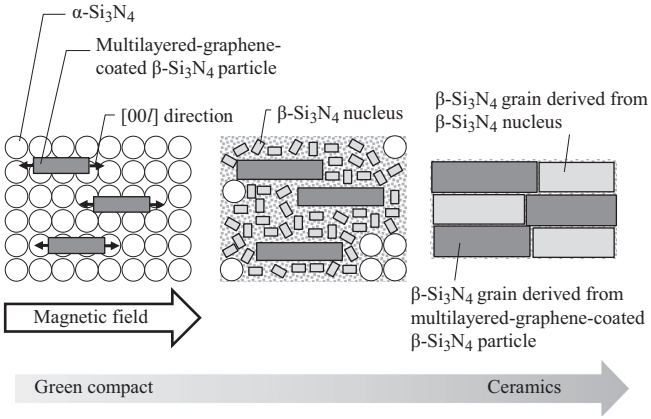

Fig. 9. Schematic illustration of formation process of *c*-axis-oriented structure.

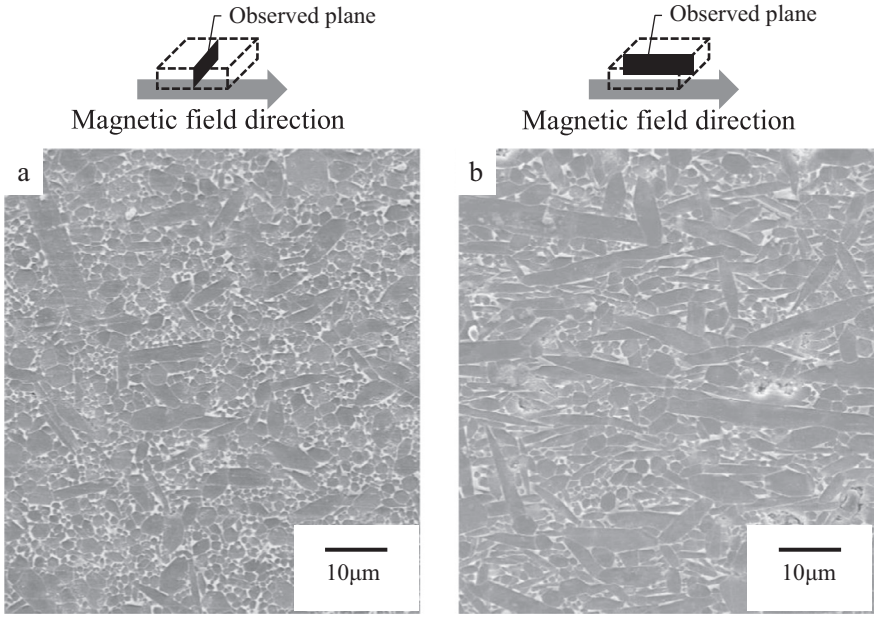

Fig. 8. Microstructures of Si_3N_4 ceramics prepared at 1 T and sintered at 1900 °C for 6 h in 0.9 MPa N_2 observed by using SEM. (a) Plane normal to the magnetic field. (b) Plane parallel to the magnetic field.

Table 1
Thermal conductivities of Si_3N_4 ceramics.

Property	Magnetic field / T	
	0	0.4
Thermal conductivity / ($W\,m^{-1}\,K^{-1}$)	77	96 (// Magnetic field) 64 (⊥ Magnetic field)

β-Si_3N_4 nucleuses. In the case of this work, initially, oriented β-Si_3N_4 particles after subjecting to multilayered-graphene removal with dispersant before the sintering process are grown along the direction parallel to the applied magnetic field. Although an external stress was not applied in the sintering process, an internal stress should occur from the anisotropic grain growth of the β-Si_3N_4 particles, resulting in a higher sintering stress along the direction normal to the applied magnetic field. The anisotropic sintering stress resulting not only from the β-Si_3N_4 particle but also from the nuclei formed by the α-β phase transformation enhanced the grain growth of β-Si_3N_4 in a direction parallel to the applied magnetic field. Finally, the highly oriented microstructure of the elongated β-Si_3N_4 grains is achieved. Thus, β-Si_3N_4 particles act as a template and cause the anisotropic sintering stress with grain growth leading to the orientation of β-Si_3N_4 grains originating from the nuclei formed by the α-β phase transformation.

Table 1 shows the thermal conductivities of Si_3N_4 ceramics prepared with and without a magnetic field of 0.4 T. Anisotropic thermal conductivity is observed between the directions parallel and normal to the applied magnetic field. The thermal conductivity obtained with the parallel direction is equal to 96 $W\,m^{-1}\,K^{-1}$, which is higher than that with the normal direction (64 $W\,m^{-1}\,K^{-1}$). In the case of non-oriented specimens, the thermal conductivity is equal to 77 $W\,m^{-1}\,K^{-1}$. Such improvement in the thermal conductivity results from the *c*-axis orientation of Si_3N_4. Consequently, the low magnetic field molding technique using multilayered-graphene-coated Si_3N_4 particles are found to be useful for preparing high thermal conductive Si_3N_4 ceramics.

4. Conclusion

In this work, we aimed at preparing multilayered-graphene-coated β-Si_3N_4 particles and fabricating *c*-axis oriented Si_3N_4 ceramics by applying a low static magnetic field and subsequent gas pressure sintering. The multilayered-graphene-coated β-Si_3N_4 particles were successfully prepared by mechanical treatment, which could be oriented even with a magnetic field of 0.4 T. The peak intensity of the G Raman band of the multilayered-graphene after the mechanical treatment process was high, implying that the crystallinity of graphene on the Si_3N_4 particles was as good as that of the raw material. The *c*-axis oriented Si_3N_4 ceramics were fabricated by applying various static magnetic fields. The thermal conductivities of the samples in the directions parallel and normal to the magnetic field were equal to 96 and 64 $W\,m^{-1}\,K^{-1}$, respectively.

Acknowledgement

This work was supported by JSPS KAKENHI Grant Numbers 26820299.

References

[1] G.C. Deeley, J.M. Herbert, N.C. Moore, Dense silicon nitride, Powder Metall. 4 (1961) 145–151.
[2] K. Komeya, F. Noda, Aluminum nitride and silicon nitride for high temperature gas turbine engines, SAE Technical Paper, 1974, p. 740237.
[3] M. Mitomo, Pressure sintering of Si_3N_4, J. Mater. Sci. 11 (1976) 1103–1107.
[4] G.R. Terwillinger, F.F. Lange, Pressureless sintering of Si_3N_4, J. Mater. Sci. 10 (1975) 1169–1174.
[5] K. Komeya, M. Komatsu, T. Kameda, Y. Goto, A. Tsuge, High-strength silicon nitride ceramics obtained by grain-boundary crystallization, J. Mater. Sci. 26 (1991) 5513–5516.
[6] M. Matsuoka, J. Tatami, T. Wakihara, K. Komeya, T. Meguro, Improvement of strength of carbon nanotube-dispersed Si_3N_4 ceramics by bead milling and adding lower-temperature sintering aids, J. Asian Ceram. Soc. 2 (2014) 199–203.
[7] I.W. Chen, A. Rosenflanz, A tough SiAlON ceramic based on alpha Si_3N_4 with a Whisker-like microstructure, Nature 389 (1997) 701–704.
[8] S.G. Guo, N. Hirosaki, Y. Yamamoto, T. Nishimura, M. Mitomo, Strength retention in hot-pressed Si_3N_4 ceramics with Lu_2O_3 additives after oxidation exposure in air at 1500 °C, J. Am. Ceram. Soc. 85 (2002) 1607–1609.
[9] C.H. Lin, K. Komeya, T. Meguro, J. Tatami, Y. Abe, M. Komatsu, Corrosion resistance of wear resistant silicon nitride ceramics in various aqueous solutions, J. Ceram. Soc. Jpn. 111 (2003) 452–456.
[10] J. Tatami, I.W. Chen, Y. Yamamoto, M. Komastu, K. Komeya, D.K. Kim, T. Wakihara, T. Meguro, Fracture resistance and contact damage of TiN particle reinforced Si_3N_4 ceramics, J. Ceram. Soc. Jpn. 114 (2006) 1049–1053.
[11] J. Tatami, E. Kodama, H. Watanabe, H. Nakano, T. Wakihara, K. Komeya, T. Meguro, A. Azushima, Fabrication and wear properties of TiN nanoparticle-dispersed Si_3N_4 ceramics, J. Ceram. Soc. Jpn. 116 (2008) 749–754.
[12] D. Kusano, G. Tanabe, S. Sato, High strength and thermal conductivity of silicon nitride for power semiconductor devices, Nikki Tech. J. 1 (2011) 1–4.
[13] K. Tsuruta, Prospects of the practical use of SiC power semiconductor devices in automotive application, Denso Tech. Rev. 16 (2011) 90–95.
[14] N. Hirosaki, S. Ogata, C. Kocer, Molecular dynamics calculation of the ideal thermal conductivity of single-crystal α- and β-Si_3N_4, Phys. Rev. B 65 (2002) 1–11.
[15] B. Li, L. Pottier, J.P. Roger, D. Fournier, K. Watari, K. Hirao, Measuring the anisotropic thermal diffusivity of silicon nitride grains by thermoreflectance microscopy, J. Eur. Ceram. Soc. 19 (1999) 1631–1640.
[16] K. Watari, K. Hirao, M.E. Brito, M. Toriyama, S. Kanzaki, Hot isostatic pressing to increase thermal conductivity of Si_3N_4 ceramics, J. Mater. Res. 14 (1999) 1538–1541.
[17] S.Q. Li, K. Sassa, S. Asai, Fabrication of textured Si_3N_4 ceramics by slip casting in a high magnetic field, J. Am. Ceram. Soc. 87 (2004) 1384–1387.
[18] X. Zhu, T.S. Suzuki, T. Uchikoshi, T. Nishimura, Y. Sakka, Texture development in Si_3N_4 ceramics by magnetic field alignment during slip casting, J. Ceram. Soc. Jpn. 114 (2006) 979–987.
[19] X.W. Zhu, Y. Sakka, T.S. Suzuki, T. Uchikoshi, S. Kikkawa, The *c*-axis texturing of seeded Si_3N_4 with β-Si_3N_4 whiskers by slip casting in a rotating magnetic field, Acta Mater. 58 (2010) 146–161.
[20] X.W. Zhu, Y. Sakka, Y. Zhou, K. Hirao, K. Itatani, A strategy for fabricating textured silicon nitride with enhanced thermal conductivity, J. Eur. Ceram. Soc. 34 (2013) 2585–2589.
[21] X. Zhu, Y. Sakka, Textured silicon nitride: processing and anisotropic properties, Sci. Technol. Adv. Mater. 9 (2008) 033001.
[22] T. Kimura, Study on the effect of magnetic fields on polymeric materials and its application, Polym. J. 35 (2003) 823–843.
[23] Y. Sakka, T.S. Suzuki, Textured development of feeble magnetic ceramics by colloidal processing under high magnetic field, J. Ceram. Soc. Jpn. 113 (2005) 26–36.
[24] C. Uyeda, K. Hisayoshi, Detection of physical coefficient of a single dust particle based on free motions caused by magnetic orientation and magnetic ejection, Space Utiliz. Res. 28 (2012) 18–22.
[25] J.F. Schenck, The role of magnetic susceptibility in magnetic resonance imaging: MRI magnetic compatibility of the first and second kinds, Med. Phys. 23 (1996) 815–850.
[26] D. Hiratsuka, J. Tatami, T. Wakihara, K. Komeya, T. Meguro, Fabrication of AlN ceramics using AlN and nano-Y_2O_3 composite particles prepared by mechanical treatment, Key Eng. Mater. 403 (2009) 245–248.
[27] S. Tasaki, J. Tatami, H. Nakano, T. Wakihara, K. Komeya, T. Meguro, Fabrication of ZnO ceramics using ZnO/Al_2O_3 nanocomposite particles prepared by mechanical treatment, J. Ceram. Soc. Jpn. 1374 (2010) 118–121.
[28] J. Tatami, H. Nakano, T. Wakihara, K. Komeya, Development of advanced ceramics by powder composite process, KONA Powder Part J. 28 (2010) 227–240.
[29] N. Hobara, K. Takizawa, A. Hagiwara, K. Sato, H. Abe, M. Naito, Effect of process parameters on electrochemical properties of mechanically prepared composite powders for solid oxide fuel cells, Adv. Powder Technol. 22 (2011) 102–107.
[30] M. Jafari, M.H. Abbasi, M.H. Enayati, F. Karimzadeh, Mechanical properties of nanostructured Al2024–MWCNT composite prepared by optimized mechanical milling and hot pressing methods, Adv. Powder Technol. 23 (2012) 205–210.
[31] K. Hosokawa, A. Kondo, M. Okumiya, H. Abe, M. Naito, One-step mechanical processing to prepare LSM/ScSZ composite particles for SOFC cathode, Adv. Powder Technol. 25 (2014) 1430–1434.
[32] J.F. Yang, G.J. Zhang, T. Ohji, Fabrication of low-shrinkage, porous silicon nitride ceramics by addition of a small amount of carbon, J. Am. Ceram. Soc. 84 (2001) 1639–1641.
[33] J.F. Yang, T. Ohji, Y.P. Zeng, S. Kanazaki, G.J. Zhang, Fabrication and mechanical properties of porous silicon nitride ceramics from low-purity powder, J. Ceram. Soc. Jpn. 111 (2003) 758–761.

[34] J. Tatami, D. Hiratsuka, S. Okada, K. Komeya, T. Wakihara, Analysis of sintering behavior of silicon nitride based on master sintering curve theory of liquid phase, J. Ceram. Soc. Jpn. 124 (2016) 375–380.
[35] C.H. Lin, K. Komeya, T. Meguro, J. Tatami, Y. Abe, M. Komatsu, Corrosion resistance of wear resistant silicon nitride ceramics in various aqueous solutions, J. Ceram. Soc. Jpn. 111 (2003) 452–456.
[36] H. Li, K. Komeya, J. Tatami, T. Meguro, Y. Chiba, M. Komatsu, Effect of HfO_2 addition on sintering of Si_3N_4, J. Ceram. Soc. Jpn. 100 (2001) 342–346.
[37] X. Zhu, T. Uchikoshi, T.S. Suzuki, Y. Sakka, Effect of polyethyleneimine on hydrolysis and dispersion properties of aqueous Si_3N_4 suspensions, J. Am. Ceram. Soc. 90 (2007) 797–804.
[38] B.K. Jang, Y. Sakka, S.K. Woo, Alignment of carbon nanotubes by magnetic fields and aqueous dispersion, J. Phys: Conf. Ser. 156 (2009) 012005.
[39] H. Hayashi, K. Hirao, M. Toriyama, S. Kanzaki, $MgSiN_2$ addition as a means of increasing the thermal conductivity of β-silicon nitride, J. Am. Ceram. Soc. 84 (2001) 3060–3062.